

CHAPTER 1

PREFLARE FEATURES IN MICROWAVES AND IN HARD X-RAYS

Ayumi ASAI, Hiroshi NAKAJIMA, Masumi SHIMOJO¹, and
Stephen M. WHITE²

¹*Nobeyama Solar Radio Observatory,
National Astronomical Observatory of Japan,
Minamisaku, Nagano, 384-1305, JAPAN
E-mail: asai@nro.nao.ac.jp*

²*Department of Astronomy, University of Maryland,
College Park, MD20742, USA*

We present a detailed examination on the nonthermal emissions during the preflare phase of the X4.8 flare which occurred on 2002 July 23. The microwave (17 GHz and 34 GHz) data obtained with Nobeyama Radioheliograph, at Nobeyama Solar Radio Observatory, National Astronomical Observatory of Japan, and the hard X-ray data taken with *Rewen Ramaty High Energy Solar Spectroscopic Imager* distinctly showed nonthermal features. We examined the temporal, spatial, and spectroscopic characteristics of the emission sources, and found loop-top sources during the preflare phase both in hard X-rays and in microwaves. Moreover, we found that the electron spectral index derived from microwave emission index closely corresponds to that obtained from the hard X-ray emission index. We also discuss the energy release mechanism in the preflare phase.

1. Introduction

Nonthermal emissions from accelerated particles are often observed in hard X-rays (HXR), γ -rays, and microwaves at the beginning of a solar flare. These nonthermal emissions are associated with intense energy release processes. The particle acceleration mechanism has been one of the most important and difficult problems in solar physics (see reviews by, e.g. Aschwanden¹). Nonthermal emissions are associated with even a small energy release process such as in a microflare². However, it has been thought that particle acceleration works efficiently only in the impulsive phase³.

On the other hand, it is also interesting to study preflare activity, since this may hold the key for understanding how the catastrophic energy release of the flare is triggered. In the preflare stage we sometimes find flare-predictive phenomena, such as a gradual enhancement of soft X-ray (SXR) emission, rise of SXR plasmoids and/or H α filaments, etc. Even in the preflare stage of a solar flare, some energy release process is probably occurring at a low level, although the energy release is much milder. It is not widely accepted that nonthermal particles are present in significant numbers prior to the impulsive phase of a flare, rather it is common to speak of preflare heating implying thermal behavior. Therefore, the reports on the nonthermal emissions during the preflare phases have been mostly negative.

Recently, Holman et al.⁴ examined the HXR features of the 2002 July 23 flare, and reported that the nonthermal energy was large even before the impulsive phase. Motivated by their work, we analyzed this flare, and found sufficient emissions both in HXR and in microwaves that can be candidates for nonthermal emissions during the preflare phase. In order to derive information on the energy release in the preflare phase, we examined in detail the features of the emission sources spatially, temporally, and spectroscopically. We report the results of the investigations of the emissions in HXR and in microwaves during the preflare phase, and discuss the relation between the nonthermal emissions and other observed phenomena.

2. Observations and Results

The intense solar flare, X4.8 on the *GOES* scale, occurred in NOAA Active Region 10039 (S12 $^{\circ}$, E72 $^{\circ}$) at 00:18 UT, 2002 July 23. This flare showed many spectacular features⁵ in HXR and γ -ray wavelengths obtained with the *Reuven Ramaty High Energy Solar Spectroscopic Imager (RHESSI)*⁶. This flare was also observed in microwaves with the Nobeyama Radioheliograph (NoRH)⁷⁹. NoRH observes the Sun in two frequencies, 17 GHz and 34 GHz, which allows us to derive a spectral index α ($F_{\nu} \propto \nu^{\alpha}$; F_{ν} is the flux at frequency ν) with a temporal resolution of 1 s. The spatial resolutions (FWHMs) of NoRH data are 14'' for 17 GHz and 7'' for 34 GHz. We synthesized the HXR images obtained with *RHESSI* by using grids 3 - 8 which gives the spatial resolution (FWHM) of about 7''. We integrated over 20 seconds to synthesize each image used in this paper. We also determined the temperature and the emission measures of the thermal plasma in the corona by using the ratios of the two of *GOES* channels. EUV images of the flare were obtained with the *Transition Region and Coronal Explorer*

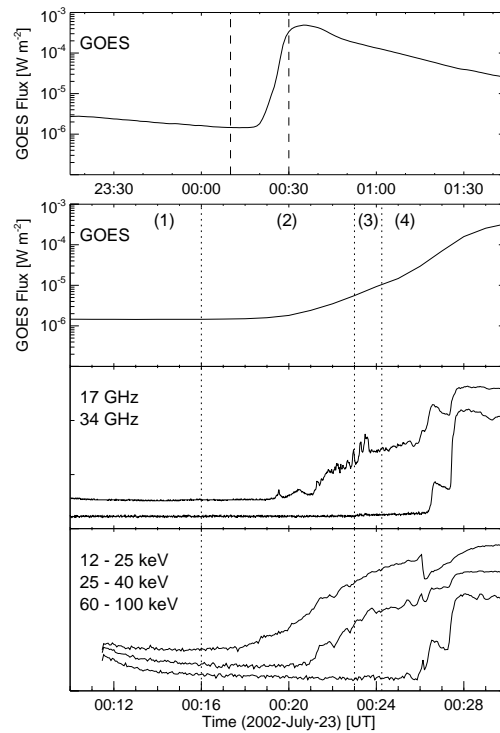


Fig. 1. Top panel: Soft X-ray flux in the *GOES* 1.0 - 8.0 Å channel of the 2002 July 23 flare. Two *dashed* vertical lines show the time range of the preflare phase. Bottom panel: Light curves of the preflare phase. From top to bottom: soft X-ray flux in the *GOES* 1.0 - 8.0 Å channel; radio correlation plot observed at 17 GHz and 34 GHz with NoRH (scaled arbitrarily); hard X-ray count rate measured with *RHESSI* in 12 - 25 keV and in 60 - 100 keV (scaled arbitrarily). The *dotted* vertical lines divide the preflare phase into four sub-phases as numbered in the top frame.

(*TRACE*^{10,11}). We used 195 Å images, in which the Fe XII line formed at ~ 1 MK is normally dominant. The pixel size of the CCD is 1''0, and the temporal resolution is about 9 s.

We focus on the nonthermal emissions in HXRs and in microwaves of the preflare phase, from about 23:00 UT, 2002 July 22 to about 00:30 UT, 2002 July 23. We divide the preflare phase into four sub-phases, and examine each phase in more detail. The bottom panel of Figure 1 shows the expanded light curves of the preflare phase of the flare (from 00:10 UT to 00:30 UT, 2002 July 23), which corresponds to the time between the

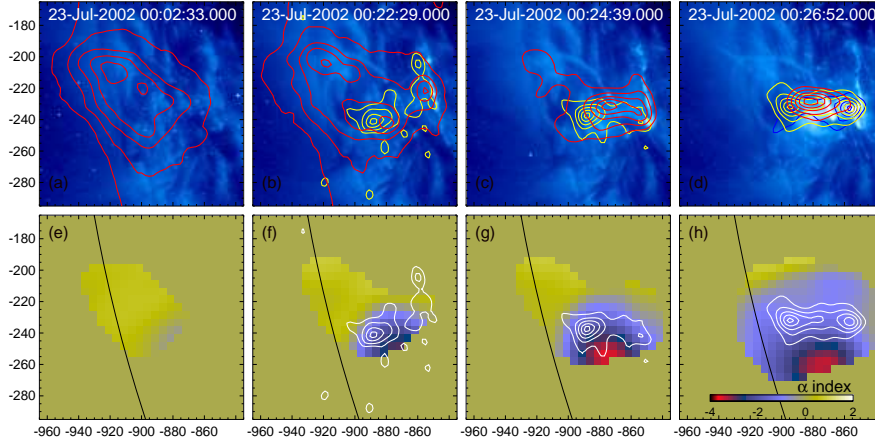


Fig. 2. Images of the flare for each phase. The top panels (a - d) show the EUV images taken with *TRACE* 195 Å. The contours show the NoRH 34 GHz brightness temperature (red), the *RHESSI* 25 - 40 keV intensity (yellow), and the 40 - 60 keV intensity (blue, only in the panel d), respectively. The bottom panels (e - h) show the maps of NoRH α index overlaid with the *RHESSI* 12 - 25 keV intensity (white). The 34 GHz contours are 15, 30, 50, 70, and 90 % of the peak intensity. Contours for the *RHESSI* HXR images are at 20, 40, 60, 80, and 95 % of the peak intensity.

dashed lines in the top panel. The time ranges of the four sub-phases are numbered at the top of the bottom panel of Figure 1.

Figure 2 shows the evolution of the flare. The top panels show the *TRACE* 195 Å images overlaid with the contour images of the NoRH 34 GHz (red), the *RHESSI* 25 - 40 keV (yellow), and the 40 - 60 keV (blue, only in the right panel), respectively. The bottom panels show the maps of NoRH α index overlaid with the *RHESSI* 12 - 25 keV intensity (white).

2.1. Before the flare (sub-phase 1)

First, we focus on the time period from about 23:30 UT, 2002 July 22 to 00:16 UT, 2002 July 23. In Figure 2a we can see a large loop-like bright region in the NoRH image⁹. We derived the spectral index α of the emission source, and found it to be within the range of -0.4 to 0.6 , which indicates that the optically-thin (free-free) thermal emission is dominant for the source. Moreover, the polarization of the sources is no more than 10 %, which eliminates the possibility of the emission from the gyroresonance near the sunspot umbrae.

The *GOES* temperature shows the existence of hot plasma even in this phase of about 5 MK. This could be related to a small flare which occurred at 22:00 UT in the same active region, although we could not confirm it due to the lack of image data for the small event. Although *TRACE* was observing the region, we cannot see any active phenomena at the time. This is presumably because the large structure is too hot to be observed in the EUV range, and we suppose that the large loop-like structure is a kind of sigmoid which is often observed at the preflare phase in SXR (see e.g. Manoharan et al.⁸).

2.2. Preflare phase (sub-phase 2)

Second, we examine the time for sub-phase 2 marked in Figure 1 (bottom panel) which includes the first flare emissions (from 00:16 UT to 00:23 UT). We can see some features of thermal emission and also clear signatures of nonthermal emission.

The *GOES* temperature rapidly increases from about 4.5 MK at 00:15 UT to above 10 MK at 00:22 UT. At the same time, the *RHESSI* count rate in 12 - 25 keV increases. Such HXR brightenings in lower energy bands, associated with a hotter *GOES* source, are often observed in a preflare phase, and the emissions are thought to be thermal. Moreover, Holman et al.⁴ performed a spectroscopic analysis of the flare with *RHESSI* data, and reported that the thermal component of the region has high temperatures up to 20 - 30 MK. After a short delay, from 00:18 UT the NoRH 17 GHz emission starts to rise, and its temporal evolution resembles the *RHESSI* 25 - 40 keV light curve. The NoRH 34 GHz emission and the *RHESSI* 40 - 60 keV count rate start to rise at 00:22 UT almost simultaneously.

Figure 2b and 2f show the images of this phase taken at 00:22:30 UT. In the *TRACE* images, we can see that a large two-ribbon structure⁹ brightens from 00:20 UT. The brightening of the ribbons implies that a larger structure rather than the core of the flare is destabilized in this phase. The *TRACE* EUV images in Figure 2b-c were taken a few minutes after this phase. We can see a diffuse loop-like structure that is identified as Fe XXIV emission from 20 MK plasma, as is often observed in *TRACE* 195 Å images during flares. A new microwave source appears above the flare ribbons at (−878, −243) arcsec heliocentric. This site corresponds to the post flare loops, which became visible in the later phase in the *TRACE* images connecting the flare ribbons. The α index is about −3.0, which implies that this source is emitting nonthermal-gyrosynchrotron radiation. The index is

quite small and shows a steep (soft) power-law spectrum. An HXR source also appeared at this site, although at slightly higher location (-890 , -240) than the microwave emission source. The HXR source is visible in both 12 - 25 keV and 25 - 40 keV bands. These sources could resemble to the “loop-top” HXR source¹². On the other hand, we can also see footpoint sources which are located on the *TRACE* flare ribbons mentioned above both in the microwave (34 GHz) and in the HXR (12 - 25, 25 - 40 keV). The energy release probably occurred in the corona, a part of which is deposited at the footpoints to produce the EUV brightenings. The HXR emissions from the flare ribbon are thought to be generated by thick-target emission by non-thermal electrons. This is an evidence for the existence of the nonthermal particles in this phase.

2.3. Ejection (sub-phase 3)

Next, we focus on the small microwave burst and the faint EUV ejection which occurred at about 00:23:30 UT. The apparent speed of the EUV ejection on the time slice image is roughly about 250 km s^{-1} . A halo coronal mass ejection (CME) associated with the flare was also observed with Large Angle Spectrometric Coronagraph (LASCO) on board the *Solar and Heliospheric Observatory* (*SOHO*: see the *SOHO* LASCO CME online catalog^a). The combination of ejections and HXR bursts has been observed in impulsive flares^{14,15,16}, and is consistent with the so-called “plasmoid-induced reconnection model”¹⁷. The plasmoid ejections correspond in detail with nonthermal emissions, and CME acceleration may also show this pattern¹⁸.

Associated with the EUV ejection, a tiny burst was observed in microwave (see the NoRH 17 GHz light curve in Fig. 1). We synthesized the images in microwaves and in HXR around the time of this peak, and examined the spectroscopic features of the coronal emission sources. Figure 3 shows the results. In the right panel we present a NoRH 34 GHz image. We overlaid the counter image with the *gray* line to show the coronal emission source. The flux spectral index α of this emission source is about -3.1 . Then, we can estimate the electron spectral index δ ($N(E) \propto E^{-\delta}$) to be about 4.8, if we assume the gyro-synchrotron emission for the microwave emission source. We also overlaid the HXR contour images on the *TRACE* (left) and NoRH (right) images with *black* lines. We performed the spectral fitting with a power law distribution for the core of the HXR emission (*black*

^aSee http://cdaw.gsfc.nasa.gov/CME_list/.¹³

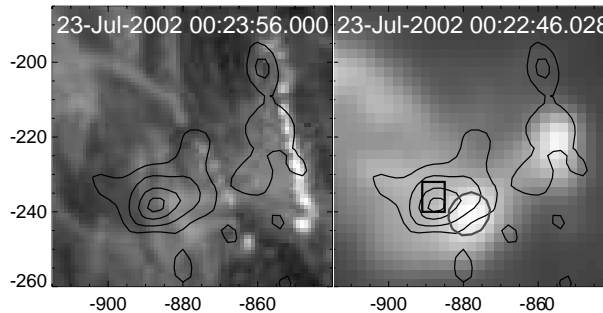


Fig. 3. *Left*: an EUV image of the flare observed with *TRACE*. *Right*: a microwave (34 GHz) image obtained with NoRH, overlaid with the counter image with the *gray* line to show the position of the coronal emission source. In both images the HXR (25 - 40 keV) counter images are overlaid with the *black* lines. The *black* box in the *right* panel shows the region used for the imaging spectroscopy.

box), and found that the spectral index γ ($I_{HXR}(\epsilon) \propto \epsilon^{-\gamma}$) is about 5.3. If we assume the thin-target model to explain the emission source, the electron spectral index δ is estimated to be 4.8, which completely corresponds to that derived from the microwave emission. These results suggest that the nonthermal electrons which generate the microwave emission sources are accelerated with the same mechanism as that for the HXR-emitting electrons.

2.4. Impulsive phase (sub-phase 4)

Finally, we examine the time after the *TRACE* ejection and before the start of the impulsive phase (from 00:24 UT to 00:27 UT). Roughly speaking, the physical features are the same as in the impulsive phase, as Krucker, Hurford & Lin¹⁹ reported. The NoRH 34 GHz source moved slightly northward ($-875, -230$), and showed a loop like structure (Figure 2c - d). Then the NoRH 34 GHz source gradually localize on the upper section of the loop. This loop structure corresponds to the most intense post-flare loop which appeared later in the *TRACE* 195 Å images. The HXR *RHESSI* 12 - 25 keV and 25 - 40 keV emissions still appear at the top of the NoRH loop. The HXR coronal sources ascend slightly as the flare progresses. A notable result is that an HXR loop-top source is observed even in 40 - 60 keV (Figure 2d). In this phase, the α index increased (became harder) to about -1.5 (Figure 2h).

3. Discussion and Summary

We examined in detail the nonthermal emissions in the preflare phase spatially, temporally, and spectroscopically. We also examined the relation between the nonthermal emissions and other observed phenomena. We identified a faint EUV ejection in the *TRACE* data which was associated with a nonthermal microwave burst, just before the fast energy release process occurred in the impulsive phase. In the phase before the ejection, we found observational evidence of both thermal and nonthermal emissions in the corona above the flare ribbon structure. Furthermore, the imaging spectroscopic analyses for the emission sources suggest that they are generated by the accelerated electrons with the same spectral indices.

Under the standard reconnection model, the current sheet reduces its thickness in the preflare phase²⁰, which leads to the fast magnetic reconnection and the violent energy release in the impulsive phase. This process is associated with the slow reconnection and/or the low-level energy release, and leads to the heating of the coronal plasma as often observed. Our results, on the other hand, indicate that the process also releases enough energy with the right conditions to accelerate particles to nonthermal energies. This suggests that energy release mechanism in the preflare phase of a typical flare may be accompanied by particle acceleration, although it is much milder than that in the impulsive phase and therefore difficult to detect in flares smaller than this event.

Acknowledgments

We first acknowledge anonymous referees for their useful comments and suggestions. We wish to thank Drs. H. S. Hudson, P. R. Lin, G. D. Holman, L. Sui for fruitful discussions and their helpful comments. We made extensive use of *TRACE* and *RHESSI* Data Center.

References

1. M. J. Aschwanden, *Space Sci. Rev.* **101**, 1 (2002).
2. A. O. Benz, & P. C. Grigis, *Adv. Space Res.* **32**, 1035 (2003).
3. S. T. Wu, et al., in *Energetic Phenomena on the Sun*, Ed. M. Kundu & B. Woodgate (NASA CP-2439, Washington DC, 1986).
4. G. E. Holman, L. Sui, R. A. Schwartz, & A. G. Emslie, A. G., *ApJL* **595**, L97 (2003).
5. R. P. Lin, et al., *ApJL* **595**, L69 (2003).
6. R. P. Lin, et al., *Sol. Phys.* **210**, 3 (2002).
7. H. Nakajima, et al., in *Proc. of the IEEE* **82**, 705 (1994).

8. P. K. Manoharan, L. van Driel-Gesztelyi, M. Pick, P. Demoulin, *ApJL* **468**, L73 (1996).
9. S. M. White, S. Krucker, K. Shibasaki, T. Yokoyama, M. Shimojo, M. R. Kundu, *ApJL* **595**, L111 (2003).
10. B. N. Handy, et al., *Sol. Phys.* **187**, 229 (1999).
11. C. J. Schrijver, et al., *Sol. Phys.* **187**, 261 (1999).
12. S. Masuda, T. Kosugi, H. Hara, S. Tsuneta, & Y. Ogawara, *Nature* **371**, 495 (1994).
13. S. Yashiro, N. Gopalswamy, G. Michalek, O. C. St. Cyr, S. P. Plunkett, N. B. Rich, and R. A. Howard, *JGR* **109**, A07105 (2004).
14. R. Kano, in *X-Ray Solar Physics from Yohkoh*, Ed. Y. Uchida, T. Watanabe, K. Shibata, & H. S. Hudson (Universal Academy Press, Tokyo, 1994), p. 273.
15. H. S. Hudson, L. W. Acton, & S. L. Freeland, *ApJ* **470**, 629 (1996).
16. M. Ohyama, & K. Shibata, *PASJ* **49**, 249 (1997).
17. K. Shibata, *Ap&SS* **264**, 129 (1999).
18. J. Zhang, K. P. Dere, R. A. Howard, M. R. Kundu, & S. M. White, *ApJ* **559**, 452 (2001).
19. S. Krucker, G. J. Hurford, & R. P. Lin, *ApJL* **595**, L103 (2003).
20. T. Magara, & K. Shibata, *ApJ* **514**, 456 (1999).